tribution of convoy electrons from solids disagree with predictions of CTC theory and with the conjecture that convoy electrons from solids originate from electrons bound in the wake of the trailing ion. It is evident from the present experimental results that further theoretical analysis of this phenomenon is required, and it is hoped that the present results will serve as a guide and stimulus.

We would like to thank the Brookhaven National Laboratory tandem accelerator staff for providing the required ion beams. We are also indebted to Dr. Krause of Oak Ridge National Laboratory for the use of the electron analyzer. One of us (R.L.) would like to acknowledge helpful discussions with N. Arista and W. Brandt of New York University. This work was supported in part by the Office of Naval Research, the National Science Foundation, and the U. S. Department of Energy.

[1]G. B. Crooks and M. E. Rudd, Phys. Rev. Lett. 25, 1599 (1970).

[2]J. Macek, Phys. Rev. A 1, 235 (1970).

[3]For a recent review of the field, see W. Meckbach, K. C. R. Chiu, H. H. Brongersma, and J. W. McGowan, J. Phys. B 10, 3255 (1977), and references cited therein.

[4]K. C. R. Chiu, J. W. McGowan, and J. B. A. Mitchell, J. Phys. B 11, L117 (1978).

[5]W. Meckbach, N. Arista, and W. Brandt, Phys. Lett. 65A, 113 (1978).

[6]C. R. Vane, I. A. Sellin, M. Suter, G. D. Alton, S. B. Elston, P. M. Griffin, and R. S. Thoe, Phys. Rev. Lett. 40, 1020 (1978), and to be published.

[7]K. Dettmann, K. G. Harrison, and M. W. Lucas, J. Phys. B 7, 269 (1974).

[8]W. Brandt and R. H. Ritchie, Phys. Lett. 62A, 374 (1977) and references cited therein.

[9]W. Brandt, in *Atomic Collisions in Solids*, edited by S. Datz, B. R. Appleton, and C. D. Moak (Plenum, New York, 1975), p. 261.

[10]H. J. Hagemann, W. Gudat, and C. Kunz, DESY Report No. SR74/7, 1974 (unpublished).

[11]We recognize that the measurement of the FWHM of a distribution that exhibits skewness introduces additional errors. However, an inspection of Fig. 1 concerning the magnitude of this error should convince the reader that the conclusions of this paper are not affected by this uncertainty.

[12]For a cusp-shaped (Ref. 7) electron velocity distribution the electron energy or velocity analyzer always measures an apparent FWHM, Γ', that is greater than the actual FWHM, Γ. We estimate $\Gamma'/\Gamma = 1 + \Delta E(4E\theta_0)^{-1}$, where $\Delta E/E$ is the FWHM of the energy resolution and θ_0 the acceptance half-angle, in radians, of the analyzer. For our analyzer, an acceptance half-angle of 1.3° and a measured energy resolution of $\leq 1\times10^{-2}$, $\Gamma'/\Gamma = 1.11$ and hence the results are within the quoted uncertainty.

Anisotropy in the Shape of the Electron-Hole-Droplet Cloud in Germanium

M. Greenstein and J. P. Wolfe
Physics Department and Materials Research Laboratory, University of Illinois at Urbana-Champaign, Urbana, Illinois 61801
(Received 1 May 1978)

Using a special infrared scanning technique we have produced photographs of the electron-hole–droplet cloud in unstressed Ge. Contrary to past beliefs, the cloud of droplets resulting from focused-laser surface excitation in neither spherical, hemispherical, nor cylindrically symmetric about the excitation point. The observed concentration of droplets along certain crystal-symmetry axes provides compelling evidence for a phonon wind which pushes droplets into the sample.

The nonequilibrium excitonic phases in semiconductors are commonly produced by surface excitation with photon energy much larger than the band gap. In high-purity germanium at low temperatures, the high-energy photoexcited carriers rapidly lose their kinetic energy by generating phonons, and within 10^{-9} sec they bind into free-exciton (FE) and electron-hole–liquid (EHL) phases.[1] These photoexcited states are conveniently studied by their characteristic LA-phonon–assisted recombination luminescence near $h\nu = 714$ and 709 meV, respectively, with lifetimes $\tau_{FE} = 2$–10 μs and $\tau_{EHL} = 40$ μs. Below 2 K and at moderate excitation levels, nearly all of the excitons have condensed into the lower-energy liquid phase.

The spatial distribution of electron-hole droplets produced by continuous point excitation has been a subject of considerable interest and importance. An argon laser beam with $h\nu = 2.41$ eV

is absorbed within about 0.02 μm of the Ge surface,[2] yet electron-hole–droplet luminescence is observed up to ~1 mm from the excitation point by slit-scan experiments.[3-5] Rayleigh-Gans scattering experiments[6] have shown that focused laser excitation produces a cloud of many droplets, each drop with dimension ~2 μm. The radial extent of the cloud increases with excitation level and is orders of magnitude larger than expected for simple diffusion of droplets from the excitation region within their 40-μs lifetime.[7]

We describe here infrared imaging experiments which give a detailed picture of the spatial distribution and time development of the electron-hole–droplet cloud in the sample. We find large anisotropies in the shape of the droplet cloud which coincide with anisotropies in both the electron-phonon deformation potential and the expected phonon flux from a point source. The data are thus interpreted in terms of a phonon wind, emanating from the excitation point, which pushes droplets into the sample.

Simple diffusion or ballistic motion of droplets into the sample can be ruled out by the experiment of Fig. 1. These data show for the first time the buildup of the electron-hole–droplet cloud just after the continuous laser excitation has been switched on. The full-width at half-maximum (FWHM) of the luminescence profile, plotted versus time in Fig. 1(b), displays an expansion rate considerably slower than the sound velocity, $v_s = 5.6\times10^5$ cm/s, and quite dependent on the laser excitation level. This is consistent with laser Doppler velocimetry measurements[8] using cw excitation. Given a carrier-phonon momentum relaxation time $\tau_p \approx 10^{-9}$ s,[9,10] these data imply that a typical force of about $F = Mv/\tau_p \approx 3\times10^{-15}$ dynes per electron-hole pair is pushing the droplets into the sample for these excitation levels. The velocity and therefore the force decrease with distance from the excitation point.

The imaging experiments are similar to that of Fig. 1 except that the image of the crystal is scanned in *two* dimensions across a small aperture while the laser continuously excites the sample. The scanning is accomplished by two galvo-driven mirrors with orthogonal axes of rotation. Luminescence light collected through the aperture passes through a spectrometer and is detected by a cooled Ge photodiode. This signal modulates the intensity of a storage oscilloscope. The x and y deflection of the scope are modulated by the galvo-drive voltages, resulting in a spatial map of the luminescence from the crystal. This technique has much better sensitivity at 1.75 μm than an infrared PbS vidicon and permits simultaneously both spectral and spatial resolution.

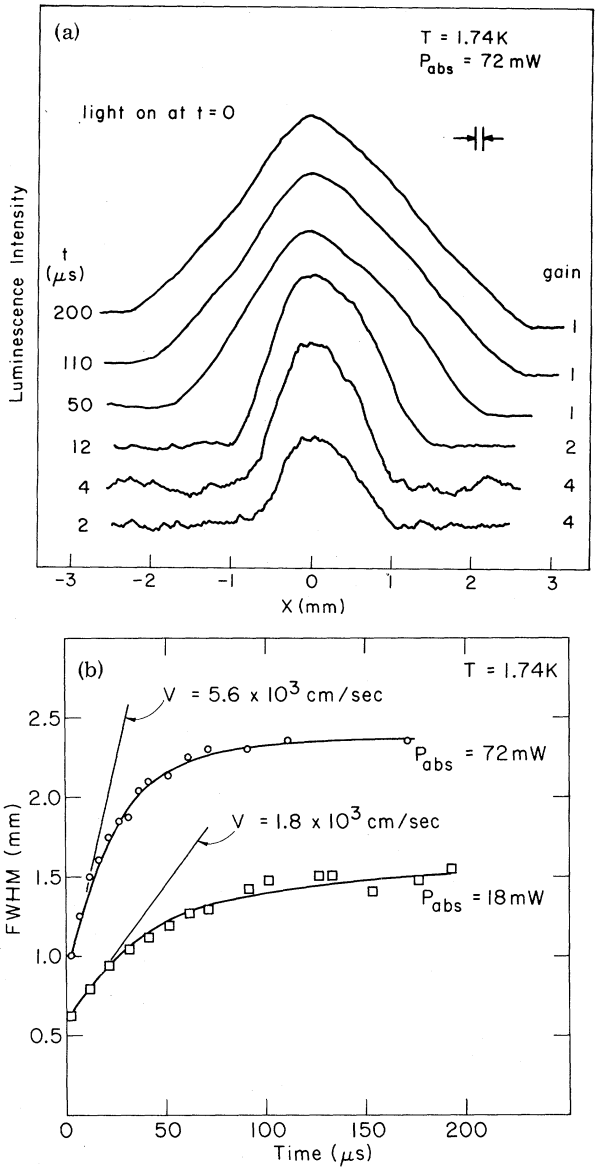

FIG. 1. (a) Time-resolved luminescence profiles showing buildup of the droplet cloud after the laser is switched on. The image of the crystal is scanned slowly across the spectrometer entrance slit for a selected boxcar delay time t and gate width 10 μs. (b) Full width at half-maxima of the profiles vs time. The rate of cloud expansion depends upon excitation level and distance from the excitation point at $x = 0$. Time resolution = 15 μs.

A photograph of the oscilloscope face is shown in Fig. 2(a). Here the crystal[11] is excited on a (100) face by a focused argon-laser beam and the

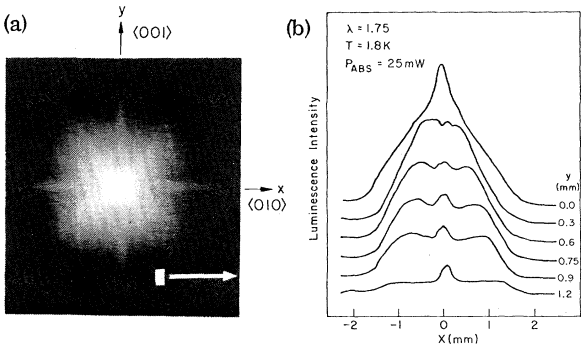

FIG. 2. (a) Photograph of the electron-hole-droplet cloud as viewed through the (100) face opposite the focused excitation. (b) Profiles obtained by scanning the crystal image in x for several y positions of the aperture, showing more quantitatively the structure of the cloud.

luminescence viewed through the opposite (100) face. This figure also shows the 709-meV luminescence profiles obtained from several x scans at different y deflections. The picture reveals striking anisotropies in the electron-hole-droplet cloud, consistent with the crystal symmetry but in contrast to previous ideas of a spherical, hemispherical, or ellipsoidal droplet distribution.

The shape of the EHL cloud is a function of laser focus and crystal orientation, as shown in Fig. 3. Figure 3(a) shows a crystal viewed through a (111) face and excited on the opposite face by a focused beam with diameter $d \approx 0.2$ mm. The distribution in Fig. 3(c) is obtained with excitation beam diameter $d \approx 2$ mm, approximately the size of the observed cloud region. Figures 2 and 3 display two major features of the cloud shape: broad "lobes" which occur along ⟨111⟩ axes extending into the crystal from the excitation point and sharper "flares" extending along ⟨100⟩ crystal axes. The flares are most apparent for sharp laser focus, whereas the ⟨111⟩ lobes more gradually lose their definition as the laser is defocused. The density and shape of the cloud is similar for excitation by a Nd-doped yttrium-aluminum-garnet laser at $h\nu = 1.17$ eV, indicating that a large fraction of the thermalization phonons from Ar-laser excitation is not involved in the cloud expansion process.[12]

The ⟨111⟩ lobes are most clearly displayed in the side view of a crystal with (100) excitation face, as shown in Fig. 4. The viewing direction, ⟨001⟩, is perpendicular to the laser beam, thus giving the third dimension corresponding to Fig. 2. This photo shows distinctly how the droplets are pushed into the crystal preferentially

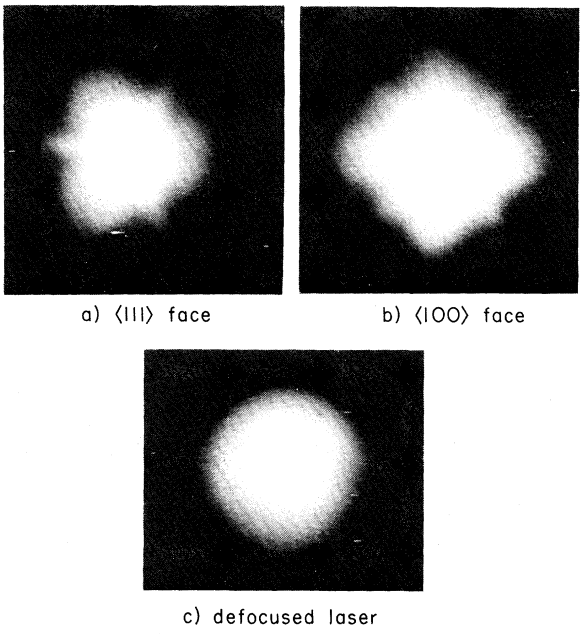

FIG. 3. (a) Photograph of a cloud produced by focused excitation of a (111) crystal face. (b) (100) face crystal with (010) axis rotated 45° from Fig. 2(a). The excitation spot is slightly larger than in Fig. 2(a). (c) Loss of structure produces by defocusing the laser beam.

along the crystal symmetry axes.

The idea that a flux of nonequilibrium phonons can push electron-hole droplets was proposed by Keldysh[13] and experimentally investigated by Bagaev *et al.*,[14] who observed a displacement of the EHL cloud by a separate source of phonons. Hensel and Dynes[9] have demonstrated that ballistic phonons generated by a heat pulse are absorbed by a cloud of droplets which was produced by volume excitation. They concluded that the

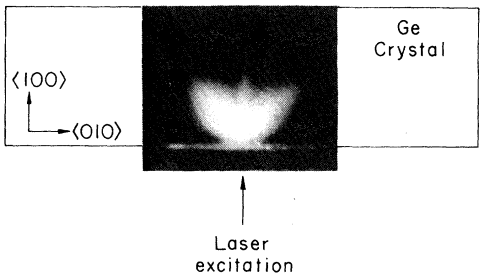

FIG. 4. Side view of the cloud showing that droplets are pushed into the crystal preferentially along ⟨111⟩ axes. The excitation face has been polished without etching to define the crystal surface better. Consequently, the droplet production efficiency is about 3× lower than Fig. 2.

longitudinal (LA) phonons traveling along ⟨111⟩ are much more strongly absorbed than transverse (TA) phonons and that droplets may be propelled several millimeters by heat pulses.

The force on a droplet due to phonon absorption depends upon the carrier-phonon coupling (i.e., absorption probability), the phonon momentum $\hbar\vec{q}$, and the phonon flux, $w(\vec{q})$. For a given phonon the absorption probability depends quadratically upon the deformation potential. For EHD in Ge, Markiewicz[15] gives expressions for the screened deformation potential E_i for electrons in the ith conduction-band valley. Figure 5(a) is a polar plot of $\sum_{i=1,4}|E_i|^2$ for longitudinal phonons propagating along directions in the (110) plane, showing a broad peak along the ⟨111⟩ axis. Results for the valence band and for transverse waves are much more nearly isotropic. In addition,[9] the absorption probability and transferred momentum increase with $\vec{q}$ up to a cutoff $2\vec{k}_F$, which is a maximum along ⟨111⟩. This contribution to the anisotropy depends in part upon the unknown energy distribution of nonequilibrium phonons.

The phonon energy flux resulting from a uniform phase-space distribution is also highly anisotropic.[16] This is because the group and phase velocities are not collinear for nonspherical $\omega(\vec{q})$ surfaces, as illustrated in Fig. 5(b). This "phonon focusing" can be described by an enhancement factor A which is the energy flux normalized to that of an isotropic medium. Statistical calculations[17] show that for LA phonons in Ge, A is a smoothly varying function of angle with a broad peak along ⟨111⟩. Maris[16] finds analytically that $A = 0.21$, 1.52, and 2.49 for

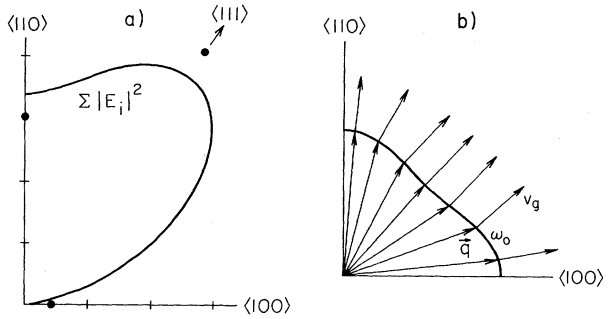

FIG. 5. (a) Polar plot of $\Sigma|E_i|^2$ in the (110) plane, displaying the large anisotropy in the deformation potential for electrons in EHD in Ge. Black dots are enhancement factors for the LA-phonon flux (arbitrary units). (b) Schematic of noncollinear phase and group velocities producing an enhanced LA-phonon flux along ⟨111⟩.

⟨100⟩, ⟨110⟩, and ⟨111⟩ directions, respectively, as plotted in Fig. 5(a). The above considerations lead us to conclude that the ⟨111⟩ lobes are produced mainly by a wind of LA phonons.

We further suggest that the flares are caused by a sharply focused flux of TA phonons. Such a distribution along ⟨100⟩ crystal axes is predicted by Maris's calculation, and has been strikingly verified in heat-pulse experiments by Hensel and Dynes.[18]

The observed anisotropies in the EHL cloud shapes are a necessary consequence of the phonon-wind hypothesis and, together with cloud buildup, velocimetry, and heat-pulse measurements, provide clear evidence for the important role of phonons in determining the electron-hole-liquid distribution in germanium.

We thank E. E. Haller for providing us with the ultrapure Ge samples and detector crystal. The deformation potential in Fig. 5(a) was computed by J. Arzegian. P. Gourley assisted in construction of the scanning system. One of us (M.G.) was supported by an Exxon fellowship. We thank R. S. Markiewicz and J. C. Hensel for useful comments. This work was supported in part by the National Science Foundation Grants No. DMR-76-01058 and No. DMR-77-11672.

[1]See reviews by T. M. Rice and by J. C. Hensel, T. G. Phillips, and G. A. Thomas, in *Solid State Physics*, edited by H. Ehrenreich, F. Seitz, and D. Turnbull (Academic, New York, 1977), Vol. 32.

[2]H. R. Phillip and E. A. Taft, Phys. Rev. 113, 1002 (1959).

[3]Ya. E. Pokrovskii and K. I. Svistunova, Fiz. Tverd. Tela 16, 3399 (1974) [Sov. Phys. Solid State 16, 2202 (1975)].

[4]R. W. Martin, Phys. Status Solidi (b)61, 223 (1974).

[5]B. J. Feldman, Phys. Rev. Lett. 33, 359 (1974); G. W. Kamerman and B. J. Feldman, Phys. Rev. B 13, 5615 (1976).

[6]M. Voos, K. L. Shaklee, and J. M. Worlock, Phys. Rev. Lett. 33, 1161 (1974); J. V. C. Mattos, K. L. Shaklee, M. Voos, T. C. Damen, and J. M. Worlock, Phys. Rev. B 13, 5603 (1976).

[7]R. M. Westervelt and B. S. Black, Bull. Am. Phys. Soc. 22, 269 (1977).

[8]J. Doehler, J. V. C. Mattos, and J. M. Worlock, Phys. Rev. Lett. 38, 726 (1977). In contrast, "ballistic expansion" with velocities exceeding v_s have been reported for strong pulsed-laser excitation: T. C. Damen and J. M. Worlock, in *Proceedings of the Third International Conference on Light Scattering in Solids, Campinas, Brazil, 1975*, edited by M. Balkanski, R. C. C. Leite, and S. P. S. Porto (Flammarion, Paris, 1976),

p. 183.
[9]J. C. Hensel and R. C. Dynes, Phys. Rev. Lett. 39, 969 (1977), and references therein; A. D. A. Hansen, thesis, University of California at Berkeley, 1977 (unpublished), for τ_p.
[10]D. S. Pan, D. L. Smith, and T. C. McGill, Solid State Commun. 23, 511 (1977).
[11]An etched $8\times8\times3$-mm^3 dislocation-free sample with $N_D - N_A \approx 2\times10^{11}$ cm^{-3}.
[12]Both thermalization- and recombination-related phonons must be considered. See also J. M. Worlock and J. Doehler, Bull. Am. Phys. Soc. 23, 422 (1978). Our photographs indicate that a significant component of the phonon wind emanates from the excitation point.
[13]L. V. Keldysh, Pis'ma Zh. Eksp. Teor. Fiz. 23, 100 (1976) [JETP Lett. 23, 86 (1976)].
[14]V. S. Bagaev, L. V. Keldysh, N. N. Sibelden, and B. A. Tsvetkov, Zh. Eksp. Teor. Fiz. 70, 702 (1976) [Sov Phys. JETP 43, 362 (1976)].
[15]R. S. Markiewicz, Phys. Status Solidi (b)83, 659 (1977).
[16]Humphrey J. Maris, J. Acoust. Soc. Am. 50, 812 (1971).
[17]B. Taylor, H. J. Maris, and C. Elbaum, Phys. Rev. B 3, 1462 (1971).
[18]J. C. Hensel, Bull. Am. Phys. Soc. 23, 421 (1978).

Ionic Model for Cr, Mn, and Fe Impurities in Cu

D. C. Abbas,[a] T. J. Aton,[b] and C. P. Slichter
Materials Research Laboratory and Department of Physics, University of Illinois at Urbana–Champaign, Urbana, Illinois 61801

(Received 3 October 1977; revised manuscript received 30 May 1978)

We report studies of the temperature dependence of the Knight shift of Cu atoms near to Cr atoms in dilute *Cu*Cr alloys. Comparison with *Cu*Mn and *Cu*Fe leads us to propose electronic structures for these important systems. We confirm the general picture of Hirst: The atoms have integral numbers of 3*d* electrons and obey Russell-Sanders coupling, but the sign of the crystal field is opposite to that of Hirst, and Fe has seven rather than six 3*d* electrons.

We report NMR studies of the temperature dependence of the Knight shift of Cu atoms near to Cr atoms in dilute *Cu*Cr alloys. The results, together with those for *Cu*Mn and *Cu* Fe, leads to a detailed picture of the electronic structure of these important systems which also accounts for the magnetic susceptibility.

Differences in a fundamental description of the 3*d* atom are at issure here. Hirst argues a single configuration $3d^n$ describes the atom, the number of 3*d* electrons being integral. There are well-defined orbital and spin quantum numbers L and S given by Hund's rules. The Friedel-Anderson picture, on the other hand, permits nonintegral numbers of *d* electrons analogous to band theories of ferromagnetism, and as usually employed does not lead to Hund's rules.

Deductions about Co in metals have been made by Narath[1] and by Dupree, Walstedt, and Warren[2] who studied the Co Knight shift and spin-lattice relaxation time. Both found that Co acts much like a Co^{2+} $3d^7$ (^4F) ion in an insulator, thus supporting the Hirst picture. Our results add Cr, Mn, and Fe to Co as 3*d* atoms which obey the Hirst picture.

In the Hirst picture[3] the orbital and spin angular moment of the magnetic atom couple to those of the conduction electron through an interaction which in general form is written

$$H_{\rm mix} = \sum_{k,m,\sigma,k',m',\sigma'} I_{kk'} a_{m\sigma}^{\dagger} a_{m'\sigma'} c_{k'm'\sigma'}^{\dagger} c_{km\sigma}, \qquad (1)$$

where $a_{m\sigma}^{\dagger}$ creates an impurity electron, $c_{km\sigma}^{\dagger}$ creates a conduction electron with a wave vector of magnitude k, and m and σ specify the z component of orbital and spin angular momenta, respectively. $I_{kk'}$ gives the strength of the interaction. The Fermi contact interaction H_F couples the conduction electrons to the neighboring Cu nuclear spins and together with $H_{\rm mix}$ produces an extra Knight shift, ΔK. We find,[4] to a good approximation,

$$\Delta K/K = g(\vec{r})\chi^S(T), \qquad (2)$$

where $\chi^S(T)$ is the spin susceptibility of the impurity. $g(\vec{r})$, which gives the spatial dependence, is independent of T. Thus measurement of ΔK enables one to deduce the temperature dependence of $\chi^S(T)$.

For *Cu*Cr we have followed the temperature variation of ΔK from 8.0 to 334 K for two neighbor shells and from 8.0 to 278 K for a third shell (Fig. 1). For *Cu* Fe[5] and *Cu*Mn[6] $\Delta K/K$ obeys a Curie-Weiss law; a plot of $K/\Delta K$ is a straight

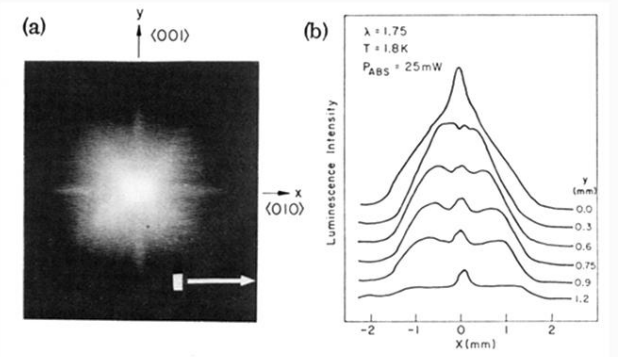

FIG. 2. (a) Photograph of the electron-hole–droplet cloud as viewed through the (100) face opposite the focused excitation. (b) Profiles obtained by scanning the crystal image in x for several y positions of the aperture, showing more quantitatively the structure of the cloud.

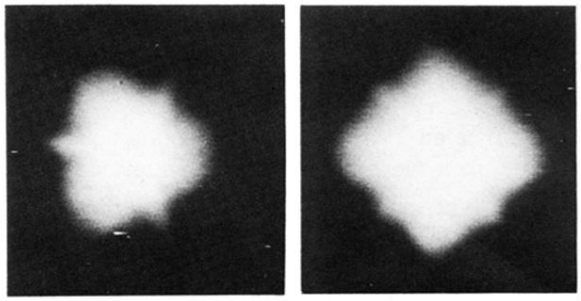

a) ⟨111⟩ face b) ⟨100⟩ face

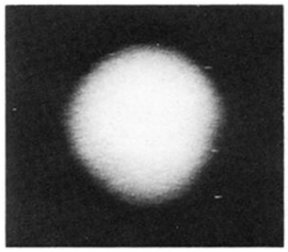

c) defocused laser

FIG. 3. (a) Photograph of a cloud produced by focused excitation of a (111) crystal face. (b) (100) face crystal with (010) axis rotated 45° from Fig. 2(a). The excitation spot is slightly larger than in Fig. 2(a). (c) Loss of structure produces by defocusing the laser beam.

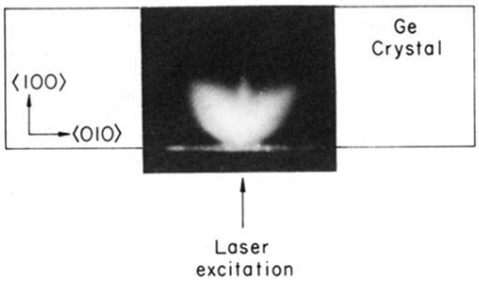

FIG. 4. Side view of the cloud showing that droplets are pushed into the crystal preferentially along ⟨111⟩ axes. The excitation face has been polished without etching to define the crystal surface better. Consequently, the droplet production efficiency is about 3× lower than Fig. 2.